



HAL
open science

Cutting tree rings into time slices: how intra-annual dynamics of wood formation help decipher the space-for-time conversion

Gonzalo Pérez-de-lis, Cyrille B K Rathgeber, Laura Fernández-de-uña, Stéphane Ponton

► To cite this version:

Gonzalo Pérez-de-lis, Cyrille B K Rathgeber, Laura Fernández-de-uña, Stéphane Ponton. Cutting tree rings into time slices: how intra-annual dynamics of wood formation help decipher the space-for-time conversion. *New Phytologist*, 2021, 233 (3), pp.1520 - 1534. 10.1111/nph.17869 . hal-04219519

HAL Id: hal-04219519

<https://hal.inrae.fr/hal-04219519v1>

Submitted on 27 Sep 2023

HAL is a multi-disciplinary open access archive for the deposit and dissemination of scientific research documents, whether they are published or not. The documents may come from teaching and research institutions in France or abroad, or from public or private research centers.

L'archive ouverte pluridisciplinaire **HAL**, est destinée au dépôt et à la diffusion de documents scientifiques de niveau recherche, publiés ou non, émanant des établissements d'enseignement et de recherche français ou étrangers, des laboratoires publics ou privés.



Distributed under a Creative Commons Attribution 4.0 International License

Methods

Cutting tree rings into time slices: how intra-annual dynamics of wood formation help decipher the space-for-time conversion

Gonzalo Pérez-de-Lis^{1,2} , Cyrille B. K. Rathgeber^{1,3} , Laura Fernández-de-Uña^{1,4}  and Stéphane Ponton¹ 

¹SILVA, Université de Lorraine, AgroParisTech, INRAE, Nancy 54000, France; ²BIOAPLIC, Departamento de Botánica, EPSE, Universidade de Santiago de Compostela, Campus Terra, Lugo 27002, Spain; ³Swiss Federal Research Institute for Forest, Snow and Landscape Research WSL, Birmensdorf CH-8903, Switzerland; ⁴CREAF, Bellaterra (Cerdanyola del Vallés), Catalonia E08193, Spain

Summary

Author for correspondence:
Gonzalo Pérez-de-Lis
Email: gonzalo.perezdelis@usc.es

Received: 2 May 2021
Accepted: 11 November 2021

New Phytologist (2021)
doi: 10.1111/nph.17869

Key words: cell enlargement, conifer, intra-ring signal, temperate forest, tracheid, tree-ring sectors, wall thickening, xylogenesis.

- Tree-ring anatomy, microdensity and isotope records provide valuable intra-annual information. However, extracting signals at that scale is challenged by the complexity of xylogenesis, where two major processes – cell enlargement and wall thickening – occur at different times and rates.
- We characterized the space-for-time association in the tree rings of three conifer species by examining the duration, overlapping, inter-tree synchronicity and interannual stability during cell enlargement and wall thickening across regular tree-ring sectors (portions of equal tangential width).
- The number of cells and cell differentiation rates determined the duration of sector formation, which augmented more rapidly throughout the ring for wall thickening than for enlargement. Increasing the number of sectors above *c.* 15 had a limited effect on improving time resolution because consecutive sector formation overlapped greatly in time, especially in narrow rings and during wall thickening. Increasing the number of sectors also resulted in lower synchronicity and stability of intermediate-sector enlargement, whereas all sectors showed high synchronicity and stability during wall thickening.
- Increasing the number of sectors had a stronger effect on enhancing time-series resolution for enlargement- than for wall-thickening-related traits, which would nevertheless produce more reliable intra-annual chronologies as a result of the more similar calendars across trees and years in wall thickening.

Introduction

In climates with marked seasonality, changing environmental conditions leave anatomically distinguishable boundaries in wood. Thanks to cross-dating, tree rings can be unequivocally assigned to a specific year, which is crucial to correctly interpreting the environmental and functional information imprinted in wood (Fritts, 1976). Although the time resolution of dated tree-ring series is annual, the signal recorded in tree rings is determined by the interaction between physiological responses to environmental conditions and developmental processes occurring at finer timescales. Intra-ring traits could be used to identify seasonal responses of tree growth processes over long time periods. Hence, there is an increasing body of research dealing with intra-ring features, including wood quantitative anatomy (Carrer *et al.*, 2017; Castagneri *et al.*, 2017), microdensity profiles (Pritzkow *et al.*, 2014; Björklund *et al.*, 2017) and stable-isotope composition (Barbour *et al.*, 2002; Helle & Schleser, 2004; Schollaen *et al.*, 2013, 2014).

In order to extract seasonal information, tree rings often have been divided according to tree-ring features, such as earlywood–latewood (Szejner *et al.*, 2018) or intra-annual density fluctuations (De Micco *et al.*, 2012; Belmecheri *et al.*, 2018). Some authors have proposed sampling specific tree-ring zones according to a targeted signal (e.g. carbon (C) and oxygen (O) isotope ratios in the last latewood segment to study fog events in *Sequoia sempervirens* (D. Don) Endl. forests; Roden *et al.*, 2009), abnormal growth features (e.g. bands of unlignified latewood cells; Piermattei *et al.*, 2020), or values of tree-ring profiles such as maximal wood density or maximal lumen area (Pritzkow *et al.*, 2014). Yet, more detailed information on the whole growing season can be obtained by dividing tree rings in cell rows or in regularly spaced sectors (Fig. 1a), and assessing the properties of each of the sectors through *in continuum* measuring techniques (De Micco *et al.*, 2012; Schollaen *et al.*, 2013, 2014). However, although spatial resolution is well-defined in these datasets (i.e. μm or number of cells), the length of the time interval at which

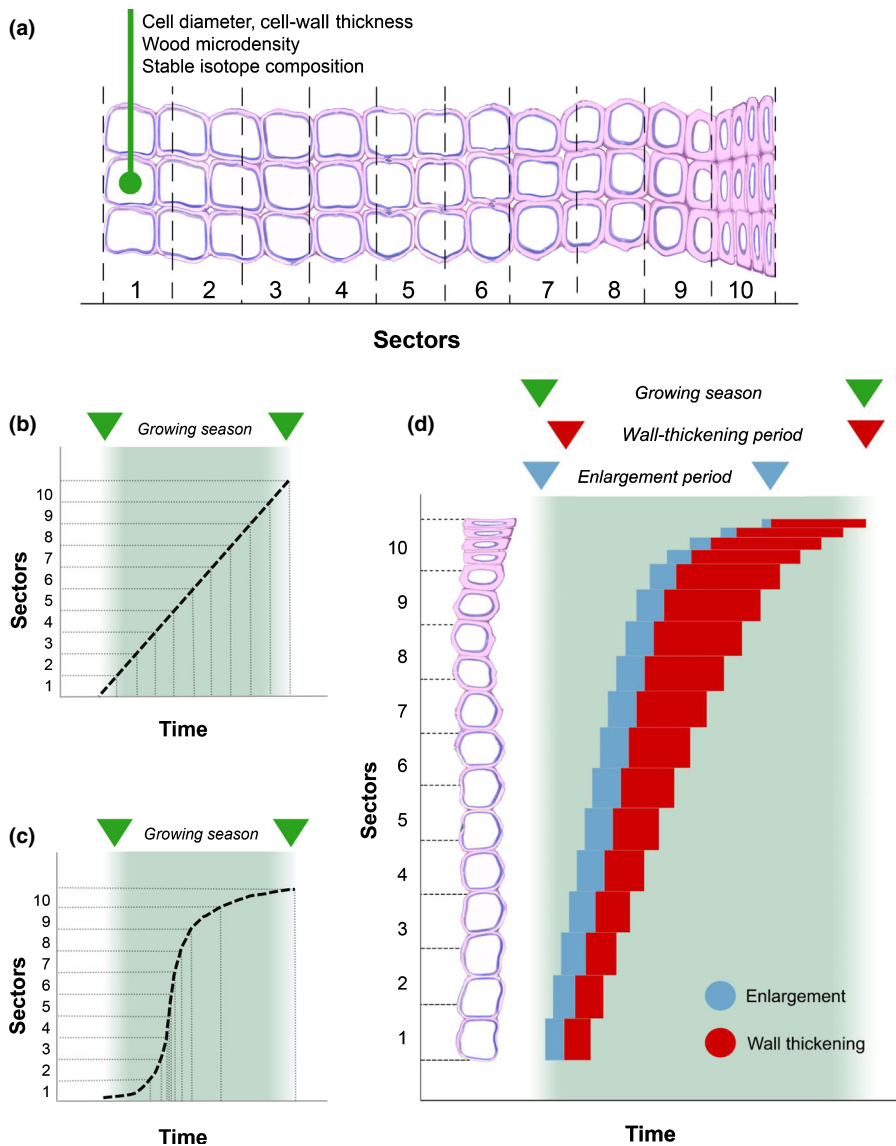


Fig. 1 Tree ring divided into regular sectors and features measured therein (a), and classical theoretical space-for-time assumptions in tree-ring science: (b) basic linear assumption; (c) sigmoidal dendrometer-based assumption; and (d) histological assumption considering xylem cell enlargement (blue bars) and wall-thickening (red bars).

environmental signals are recorded in each spatial unit within the ring (i.e. time resolution) is largely unknown.

Environmental conditions can be imprinted in tree rings in a particular time window during cell differentiation (Rathgeber *et al.*, 2016). Before becoming functional, xylem mother cells follow a succession of differentiation phases: cell enlargement, wall thickening and lignification, and, finally, programmed cell death. The timing of cell differentiation has been assessed through repeated observation of anatomical sections, particularly in conifers thanks to their homogeneous wood structure (composed mainly of tracheids). However, intra-annual growth processes cannot be assessed retrospectively from mature rings. Long intra-ring records thus must be dated through a retroactive space-for-time conversion based on the radial position of the measures. In some cases, it is assumed that xylem cells are formed one after the other following a linear pattern (Fig. 1b), whereby the growing season is divided into discrete time intervals whose duration is proportional to the number of cells (Popkova *et al.*, 2018) or the

sector width (Schollaen *et al.*, 2013, 2014; Szymczak *et al.*, 2019). Other authors have inferred the timing of sector formation through correlative analyses between a chronology of intra-ring parameters and monthly climate records (Carrer *et al.*, 2016, 2017; Castagneri *et al.*, 2017; Belokopytova *et al.*, 2019). However, dating intra-ring chronologies would require that equivalent sectors (i.e. sectors of the same rank) produced in different trees and years were formed during a similar time window, but whether this correspondence exists is largely unknown despite the increasing interest in synchronic interannual growth patterns across populations (Shestakova *et al.*, 2016).

Short-term dendrometer surveys also have been used to date intra-ring isotope (Barbour *et al.*, 2002), wood anatomy (Pacheco *et al.*, 2018) and wood microdensity (Bouriaud *et al.*, 2005) records, by inferring intra-annual changes in cell division rates and the time required for intra-ring sectors to enlarge (Ogée *et al.*, 2009; Schollaen *et al.*, 2014; Soudant *et al.*, 2016). Although this approach accounts for the fact that environmental

information is integrated in wood in a nonlinear way (Fig. 1c), some concerns have been raised regarding its use to date tree-ring isotope records (Monson *et al.*, 2018). Growth in volume and in biomass have been shown to be decoupled (Cuny *et al.*, 2015), which places two alternative timescales on intra-annual series of tree-ring features (Fig. 1d). In addition, differentiation phases frequently comprise several cell rows simultaneously, suggesting that tree-ring cells are not formed in separate time windows but instead in overlapping time intervals. For these reasons, xylogenesis data increasingly have been used to date intra-ring isotope records (Treydte *et al.*, 2014; Belmecheri *et al.*, 2018; Fonti *et al.*, 2018). However, temporally unstable tree phenology and wood formation rates could undermine the use of short-term xylogenesis data to interpret long intra-ring series. A detailed study of the association between space and time within tree rings therefore is required to better understand the information obtained at the intra-annual scale in tree-ring science (Pritzkow *et al.*, 2014; Schollaen *et al.*, 2014; Monson *et al.*, 2018).

In conifers, cell counts obtained weekly from wood microsections can be used to compute wood formation kinetics at the site level, encompassing the timing, rate, and duration of enlargement and wall thickening for each tracheid within a tree ring (Cuny *et al.*, 2013, 2014). Here, this approach is developed further to investigate the association between space and time within tree rings using data from three sites located in the Vosges Mountains (northeastern France), where three coexisting conifer species (silver fir (*Abies alba* Mill.), Norway spruce (*Picea abies* (L.) H. Karst.) and Scots pine (*Pinus sylvestris* L.)) were monitored over a 3-yr period (Cuny *et al.*, 2014). For this purpose, we combined quantitative wood anatomy data with estimations of timings of tracheid differentiation based on an empirical model of wood formation dynamics in order to date the formation of different intra-ring sectors. Three main scientific questions were addressed for the enlargement and wall-thickening phases: (1) Are regular sectors formed in separate time windows of the same duration? (2) How does the number of sectors (sector frequency) affect time resolution in tree rings? and (3) Can individual intra-ring series based on regular sectors from different trees and years be pooled together to build representative chronologies?

Materials and Methods

Dataset characteristics

We used xylogenesis data from three sites located between 350 and 700 m above sea level in the Vosges mountains (northeastern France) (Cuny *et al.*, 2014). The climate of the study area is temperate with continental influence. The mean temperature for the period 1961–1990 was 8.3°C with a mean annual precipitation of 1315 mm. The 2007–2009 period was slightly warmer than average, and the amount of precipitation ranged from 1508 mm in 2007 to < 1200 mm during the two following years. Mean temperature in 2007–2009 was higher at the low-elevation site (P3: 10.3°C) than at the intermediate (P2: 9.2°C) and high-elevation (P1: 8.6°C) sites ($F = 18.423$, $P < 0.001$), whereas mean annual precipitation was 1741 mm at P1, 1149 mm at P2

and 998 mm at P3 ($F = 37.435$, $P < 0.001$; Supporting Information Fig. S1).

For each stand, 15 individuals belonging to the three study species (five per species) were monitored between 2007 and 2009. Each week, from April to November, a microcore was taken from the stem of each tree at *c.* 1.3 m aboveground using a Trephor[®] tool (Vitzani, Belluno, Italy). Microcores were dehydrated and embedded in paraffin before 5–10- μ m-thick transverse sections were cut and stained with cresyl violet acetate. See Cuny *et al.* (2012) for further details about sample collection and processing.

A transmitted light microscope equipped with a polarizing filter (AxioImager.M2; Zeiss) was used to count the number of enlarging, wall-thickening and mature tracheids along at least three radial files in each cross-section. Tracheid lumen diameter and shape were used to distinguish enlarging cells from the narrower cambial cells, whereas birefringence of secondary walls under polarized light was used to identify wall-thickening and lignifying cells (hereafter referred as wall-thickening cells solely). Mature tracheids were determined by their empty lumens and their lignified walls, which appear uniformly blue (Cuny *et al.*, 2012). The number of cells per differentiation phase from the three radial files were averaged, and then standardized according to the number of cells in the previous ring using the R package CAVIAR (Rathgeber *et al.*, 2018). In addition, tracheid dimensions (i.e. cell radial diameter and cell-wall thickness) were measured on digital images of mature tree rings (samples taken at the end of the growing season) on at least three radial files per tree and year using the software WINCELL (Regent Instruments, Québec, QC, Canada) (see Cuny *et al.*, 2014, for details).

Assessment of the timing of sector formation

Generalized additive models (GAMs) were used to fit the weekly cell counts per differentiation zone for each tree and growing season (Fig. 2a). Enlarging and wall-thickening cell counts were fitted using GAMs with a quasi-Poisson distribution (Wood, 2006). However, because mature cells accumulate along the growing season until reaching a plateau once the ring is completed, the accumulation of mature cells was fitted using shape-constrained additive models (SCAMs) with a quasi-Poisson distribution (Pya & Wood, 2014). In a similar way to the approach described by Cuny *et al.* (2013) for stand-level calculations, tree-level GAMs and SCAMs were used to predict the counts of enlarging (EZ), wall-thickening and lignifying (WZ), and mature (MZ) cells for each day of the year (DOY). The cumulative sums of differentiating and mature cells (EWMZ, WMZ and MZ) then were calculated, and new SCAMs were fitted to the obtained curves. The EWMZ curve was used to derive the cell entry rates (eR) into the enlargement zone (i.e. cell division rates) in each date by using the equation from Cuny *et al.* (2013). The inverse functions of these models were used in turn to compute the timings of tracheid differentiation phases. Hence, using this approach we estimated the dates for the beginning and cessation of enlargement (bE_i and cE_i , respectively) and wall thickening (bW_i and cW_i , respectively) for each 'virtual cell' i in the ring (Fig. 2b). For a given cell i , cE_i was assumed to be concurrent

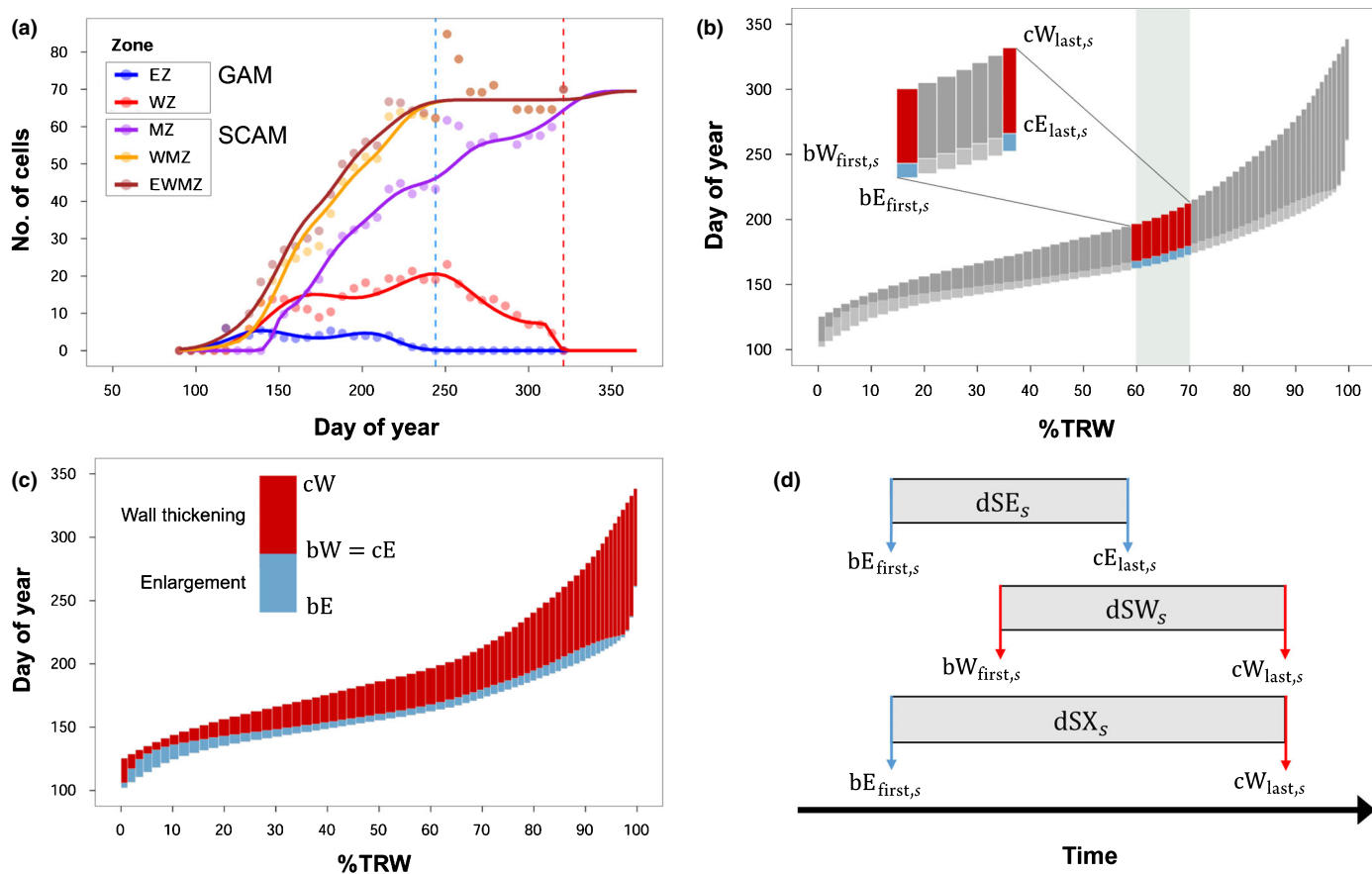


Fig. 2 Illustration of the methodology used to date xylem cell residence times in differentiation phases (a, b) and tree-ring sectors formation (c, d). (a) Example of fitting of generalized additive model (GAM) and shape-constrained additive model (SCAM) on series of weekly cell counts for EZ (cell enlargement), WZ (wall thickening), MZ (mature), WMZ (wall-thickening + mature), and EWMZ (cell enlargement + wall-thickening + mature) zones for one individual and year. Cell timings are computed using the cumulative curves MZ, WMZ and EWMZ, and dates of cessation of tree-ring enlargement (blue dashed line) and maturation (red dashed line). (b) Resulting durations of cell enlargement (blue bars, dE) and wall thickening (red bars, dW) according to cell position along the ring. bE , date of the beginning of cell enlargement; cE , date of cessation of cell enlargement; bW , date of the beginning of cell-wall thickening; cW , date of cessation of cell-wall thickening. (c) Illustration of the data used to compute the duration of enlargement (dSE), wall thickening (dSW) and both processes (dSX) of a sector (background shadow). $bE_{first,s}$, date of the beginning of enlargement of the first-born cell in a sector; $bW_{first,s}$, date of the beginning of wall thickening of the first-born cell in a sector; $cE_{last,s}$, date of cessation of enlargement of the last-born cell in a sector; $cW_{last,s}$, date of cessation of wall thickening of the last-born cell in a sector; %TRW, percentage of the final tree-ring width. (d) Illustration of the overlapping between the different periods of differentiation within a sector.

with bW_i , whereas cW_i was equivalent to full tracheid maturation (Table S1). The residence time of a cell i in enlargement was defined as $dE_i = cE_i - bE_i$, whereas that of wall thickening was given by $dW_i = cW_i - bW_i$ (Fig. 2b). Models were developed using the packages R/MGCV (Wood, 2006) and R/SCAM (Pya & Wood, 2014) for GAM and SCAM calculations.

Morphological measurements of individual xylem cells were used to associate the time of development of each sector with its location into the ring. As the total number of cells measured on the anatomical sections did not always coincide exactly with that estimated by the SCAMs, we used the relative position of the measured tracheids to match both datasets (Fig. 2b). Because the intra-ring resolution more frequently used in dendro-isotopic and dendro-anatomical studies is the sector, not individual cells, tree rings were divided into evenly spaced sectors. Each cell row then was assigned to a sector according to its position. For a ring divided into, for example, 10 sectors, the first consecutive cells whose cumulative length was

within the 10th percentile of the total tree-ring width were assigned to the first sector, whereas those between the 10th and 20th percentiles were assigned to the second sector, and so on (Fig. 2c). Tracheids at the boundary between two sectors were assigned to the sector containing their geometric centre.

Computation of the duration of sector formation

The periods of enlargement and wall thickening were computed for each sector according to the onset and cessation of each phase (Fig. 2d). The time taken by all of the cells within a sector to complete their enlargement (dSE) then was assessed as:

$$dSE_s = cE_{last,s} - bE_{first,s} \quad \text{Eqn 1}$$

($bE_{first,s}$, date of the beginning of the enlargement of the first-born cell of the sector s ; $cE_{last,s}$, date of the end of the enlargement

of the last-born cell in s). A similar approach was used to compute the duration of wall thickening for a sector (dSW):

$$dSW_s = cW_{last,s} - bW_{first,s} \quad \text{Eqn 2}$$

($bW_{first,s}$ date of the beginning of the wall thickening of the first-born cell in s ; $cW_{last,s}$ date of the end of the wall-thickening of the last-born cell in s). The total duration of sector formation (dSX) was calculated as:

$$dSX_s = cW_{last,s} - bE_{first,s} \quad \text{Eqn 3}$$

At the time of formation, sectors can contain both enlarging and wall-thickening cells. Hence, unlike at the cell level, bW_{first} is not concurrent with cE_{last} . In addition, we assessed the average residence times in number of days for enlarging (dE) and wall-thickening (dW) cells for all of the sectors, along with the number of cells per sector (nC), mean cell entry rates into the enlargement phase (eR), mean cell diameter (CD), mean cell-wall thickness (CWT) and total ring cell number (RCN). The first predicted date of the first-sector enlargement (bE_1) was identified as the beginning of xylem enlargement (Table S1).

Sector overlapping, inter-tree synchronicity and interannual stability calculation

In order to evaluate whether successive tree-ring sectors overlapped in time, we analyzed the daily variation on the number of sectors simultaneously containing either enlarging or wall-thickening cells, being counted and expressed as the percentage of overlapping sectors per DOY. The maximum number of time-overlapped sectors then was extracted for each tree.

We calculated inter-tree synchronicity of equivalent sectors among trees within a year (i.e. common sector formation period of each tree and the mean of all the trees of the same species across sites), as well as interannual timing stability across years in each tree (i.e. common sector formation period of each year and the mean of the 3 yr within a tree).

The respective periods of enlargement (SE) and wall thickening (SW) in a given sector s , year y and tree i were intervals denoted by $S_{syzi} = [b_{first,syi}, c_{last,syi}]$, where $b_{first,syi}$ represents the beginning of a phase ($bE_{first,syi}$ for enlargement, $bW_{first,syi}$ for wall thickening) in the first-born cell, whereas $c_{last,syi}$ is the cessation ($cE_{last,syi}$ for enlargement, $cW_{last,syi}$ for wall thickening) in the last-born cell. In the same manner, the mean period for a given sector s and year y in all the trees for each species was given by:

$$Smean_{syz} = \left[\frac{1}{t} \sum_{i=1}^t b_{first,syzi}, \frac{1}{t} \sum_{i=1}^t c_{last,syzi} \right] \quad \text{Eqn 4}$$

(t , total number of trees per species ($t = 15$)). The common interval (CI) for either enlargement or wall thickening was defined as $CI_{syi} = S_{syi} \cap Smean_{syz}$, which is the intersection between the period in each tree i and the corresponding mean period at the species level. Finally, synchronicity (Syn) of either enlargement

or wall thickening of a given sector s , year y and tree i was calculated as follows:

$$Syn_{syi} = \frac{CI_{syi}}{S_{syi}} \times 100 \quad \text{Eqn 5}$$

(CI_{syi} , duration of the common interval for sector s ; S_{syi} , duration of sector s (Fig. S2)). The same approach was used to evaluate the stability in timing over n yr ($n = 3$), which was called, by extension, interannual stability. The average for each tree i over n yr was used as the corresponding mean period ($Smean_{si}$) to calculate the interannual stability index (Fig. S2).

Sector overlapping, inter-tree synchronicity and interannual stability were simulated for a ring divided into 5, 10, 16 (instead of 15 to avoid irrational numbers in sector relative width) and 20 regular sectors. Sector overlapping also was examined at the cell and tree-ring width levels.

Data analysis

In order to ascertain the drivers of sector formation timespan (dSE, dSW and dSX), we compared the effects of individual cell residence times (dE, dW), cell division rates (eR), number of cells (nC), species and site along a ring divided into 10 regular sectors through generalized linear mixed models with a Gamma error distribution. We used a log-link function for the dSE model, whereas an identity link function was applied in the dSW and dSX models. Up to eight narrow rings that could not be divided into 10 regular sectors containing at least one tracheid in radial direction were discarded from sector duration analyses ($n = 127$ rings).

Generalized linear mixed models were used to test the effect of variable sector frequency, RCN, mean ring CD and CWT on maximum overlapping. We included CD as a predictor in the sector enlargement model because it is acquired through enlargement (Cuny *et al.*, 2014), whereas the wall-thickening model included both CD and CWT, following findings by Björklund *et al.* (2017). Linear mixed-effects models were used to assess the relative effect of the first-sector enlargement onset (bE_1), cell residence times (dE, dW), cell division rates (eR), number of cells (nC) and variable sector frequency on inter-tree synchronicity and interannual stability across the ring. In order to ensure proper pairwise comparisons, 27 rings that could not be divided into 20 regular sectors containing at least one cell were discarded for sector overlapping and inter-tree synchronicity analyses ($n = 108$ rings), whereas an additional six trees with data available for only 1 yr were not considered in the interannual stability analysis ($n = 102$ rings).

The R package LME4 was used to adjust all of the mixed models (Bates *et al.*, 2015). The random effects structure of the models included the factors 'Tree' and 'Year', selecting the simplest among those minimizing Akaike's Information Criterion scores (tolerance ≤ 2). Relative importance of fixed effects in the mixed models was evaluated by comparing their respective sum of squares (SS), calculated using R/LMTEST (Kuznetsova *et al.*, 2017), whereas multiple comparisons across factor levels were

performed with R/MULTCOMP (Hothorn *et al.*, 2008). Marginal and conditional R^2 for mixed-effect models were estimated following the method proposed by Nakagawa & Schielzeth (2013). Potential multicollinearity problems in models were checked through the variance inflation factor. Differences across species, sites and years regarding wood phenology, dynamics of xylogenesis and tree-ring features in the entire population ($n = 135$ rings) were assessed complementarily through an ANOVA. Standard errors were calculated to show the variance of the results included in text, tables and figures. All analyses were carried in R v.3.5.0 (R Core Team, 2017).

Results

Wood phenology and tree-ring features

The period of xylem formation comprised on average 191 ± 4 d in pine and 190 ± 4 d in fir, but only 179 ± 4 d in spruce ($F = 3.331$, $P = 0.04$). Trees at the low-elevation site (P3) had an earlier onset of xylem enlargement (bE_1) and a later cessation of xylem maturation than those at higher sites (P1 and P2). The duration of the wood formation period was in tune with the total amount of cells produced (RCN, $r = 0.63$, $P < 0.001$). Mean RCN (tree-ring width, TRW) varied from 73.4 ± 6.7 cells ($2544.4 \pm 238.0 \mu\text{m}$) in fir to 60.0 ± 4.8 cells ($1922.5 \pm 158.4 \mu\text{m}$) in spruce and 43.2 ± 4.1 cells ($1309.8 \pm 120.0 \mu\text{m}$) in pine. Mean CD was inversely correlated to the proportion of latewood ($r = -0.62$, $P < 0.001$), which was positively correlated with mean CWT within a ring ($r = 0.68$, $P < 0.001$). Higher RCN occurred at P3, whereas the highest mean CD and lowest mean CWT were noted at P1 ($P < 0.001$; Table S2). Differences in TRW, RCN, CD and CWT across years were negligible (Table S2). RCN was highly correlated with mean cell division rates (eR, $r = 0.91$, $P < 0.001$), but inversely correlated with cell enlargement residence times (dE, $r = -0.69$, $P < 0.001$).

Tracheid morphology varied from earlywood (i.e. thin walls and wide lumen) to latewood (i.e. thick walls and narrow lumen), as shown by the CWT : CD ratio varying from $5.6 \pm 0.1\%$ to $30.0 \pm 0.8\%$ in a ring divided into 10 regular sectors (Fig. 3a). The number of xylem cells per sector (nC) steadily increased throughout the ring (Fig. 3b), with a sharp increment in the last sector for fir ($\leq 14.1 \pm 1.0$ cells) and spruce ($\leq 11.6 \pm 0.8$ cells), and less markedly for pine ($\leq 7.9 \pm 0.6$ cells). Directly correlated with nC ($r = 0.48$, $P < 0.001$), eR dropped in the last sector (0.23 ± 0.02 cells d^{-1} ; Fig. 3c), varying across species (fir > spruce > pine) and sites (P3 > P2 > P1) (Table S2). The maximum eR within the ring was strongly correlated with RCN ($r = 0.85$, $P < 0.001$).

Changes in the duration of sector formation along the ring

Although mean cell enlargement residence time decreased by half along a ring divided into 10 regular sectors ($dE_1 = 11.9 \pm 0.7$ d and $dE_{10} = 5.8 \pm 0.8$ d; Fig. 3d), the duration of sector enlargement peaked in the last sector (on average, $dSE_1 = 21.4 \pm 1.2$ vs $dSE_{10} = 51.4 \pm 2.6$ d; Fig. 3e). By contrast, the three- to four-fold increase

in cell residence times in the wall-thickening phase along the ring (on average, $dW_1 = 13.6 \pm 0.7$ d and $dW_{10} = 46.9 \pm 2.4$ d; Fig. 3d) was akin to that for the duration of sector wall thickening (on average, $dSW_1 = 26.4 \pm 1.4$ and $dSW_{10} = 76.3 \pm 2.7$ d; Fig. 3e), also being comparable to the two- to three-fold increase experienced by total duration of sector formation along a ring (on average, $dSX_1 = 36.3 \pm 1.4$ d and $dSX_{10} = 82.8 \pm 2.9$ d; Fig. 3e).

Sectors bearing more cells (nC) with longer residence times and lower cell division rates (eR) had longer durations in all the phases. However, whereas variance in dSE was explained mainly by eR and nC (Table 1), that in dSW and dSX was influenced more by the cell wall-thickening residence times (dW; Table 1). Interestingly, pines showed longer dSE than firs and spruces, except in the last sector (Table 1; Fig. S3).

Evolution of sector overlapping along the growing season

The maximum proportion of xylem cells experiencing simultaneous wall thickening (on average, $32.7 \pm 0.6\%$ of cells, $47.5 \pm 2.0\%$ of TRW) was higher than the one experiencing enlargement (on average, $12.4 \pm 0.5\%$ of cells, $20.2 \pm 0.6\%$ of TRW), in accordance with the longer duration of wall thickening (Fig. 3 vs Fig. 4). The daily proportion of enlarging sectors peaked in May, coinciding with the highest proportions of enlarging cells and TRW (Fig. 4a). Despite the proportion of wall-thickening cells and TRW peaking in late September (late August) in fir and pine (spruce), the maximum % of wall-thickening sectors in a ring divided into 5–20 regular sectors had already been attained in June and remained rather constant for 2–3 months (Fig. 4b).

Models showed that trees producing fewer cells over the year (low RCN) had more overlapped sectors regardless of the phase, although its relative importance was higher during enlargement (see SS in Table 2; Fig. S4). At cell enlargement, pines showed more overlapped sectors than the other species. However, although CD was not related to higher sector overlapping, rings with high mean CWT had more overlapped sectors (Table 2). Sector frequency affected the percentage of overlapped sectors throughout the year (Fig. 4). The maximum percentage of overlapped sectors decreased > 19% for both phases as sector frequency increased from 5 to 16 sectors (Table 2; Figs S4, S5). Differences between 16 and 20 regular sectors were negligible for both phases, however.

Inter-tree synchronicity and interannual stability in sector formation

For 10 sectors, the formation of the first two to four sectors was highly synchronous among trees of the same species for both enlargement and the wall-thickening period (Fig. 5a), despite trees being located across three study sites at different altitudes (Fig. S6). In subsequent sectors, however, synchronicity remained high for wall thickening (on average, 75% in fir, 77% in spruce and 81% in pine; Fig. 5a) but decreased for enlargement, especially in fir (29% for Sector 8). The comparison, within each tree, of equivalent sectors over the three study years (i.e. interannual stability) showed that the timing of wall

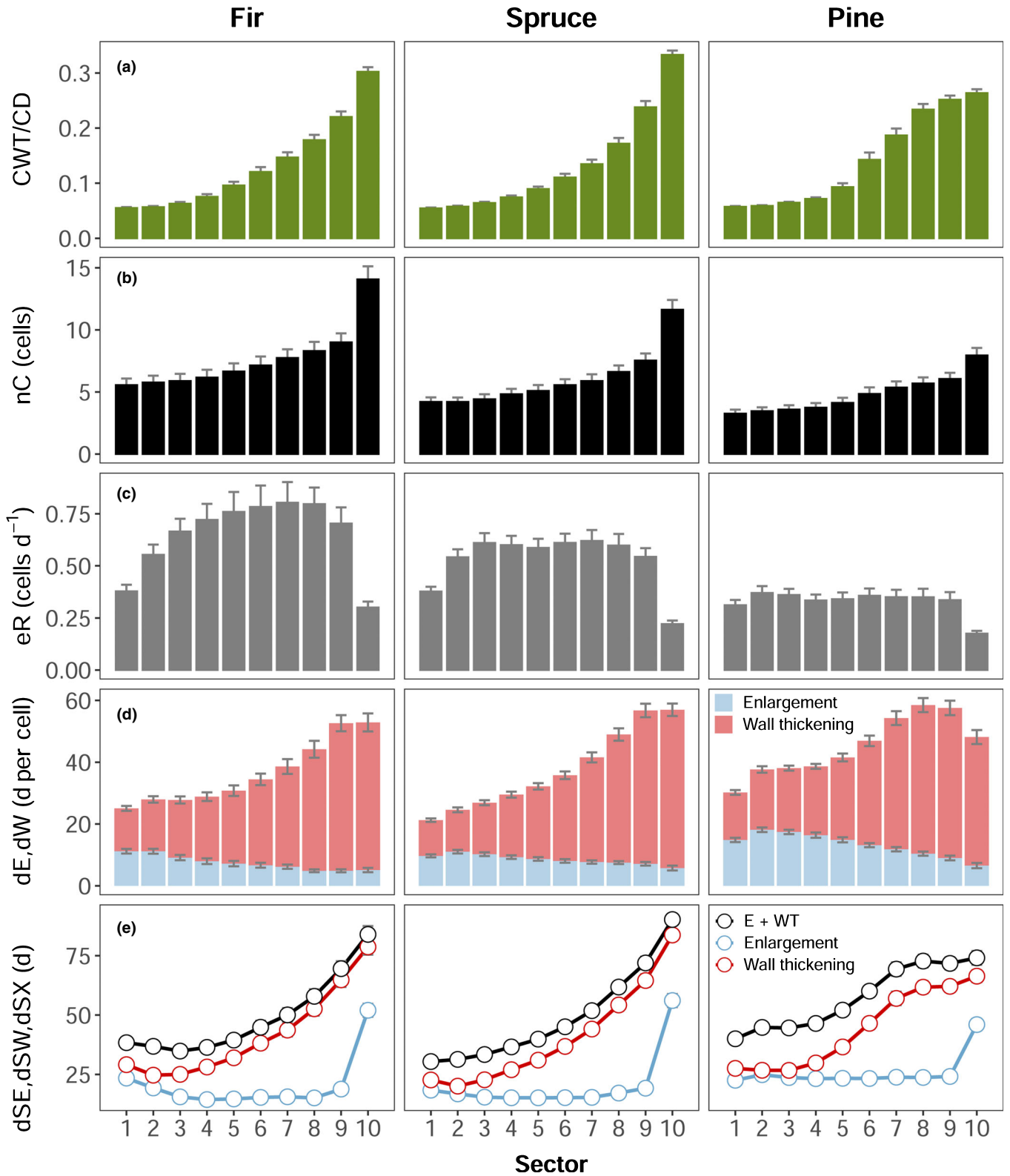


Fig. 3 Structural and time characteristics of tree-ring sectors in silver fir, Norway spruce and Scots pine: (a) Ratio between cell wall thickness (CWT) and cell diameter (CD); (b) mean number of cells per sector (nC); (c) mean cell division rates (eR); (d) mean cell residence time for enlargement (dE, blue bar) and wall-thickening (dW, red bar) phases; and (e) duration of enlargement (dSE, blue line), wall thickening (dSW, red line) and entire formation (dSX, black line) per sector. Mean \pm SE values are shown for each study species.

Table 1 Generalized linear mixed models for the sector enlargement (dSE), wall-thickening (dSW) and entire formation (dSX) timespans ($n = 127$ rings).

Fixed effects	df	Enlargement (dSE)		Wall thickening (dSW)		Entire formation (dSX)	
		Est (SE)	SS	Est (SE)	SS	Est (SE)	SS
Intercept		2.931 (0.031)		41.142 (0.697)		50.868 (0.527)	
nC	1	0.489 (0.012)	53.869	7.661 (0.303)	43.997	7.434 (0.277)	13.565
eR	1	-0.384 (0.008)	169.046	-3.727 (0.150)	29.934	-3.695 (0.139)	34.407
dE	1	0.198 (0.009)	28.537			4.974 (0.163)	4.900
dW	1			18.370 (0.193)	157.722	18.617 (0.179)	100.831
Species	2		1.289		0.094		0.128
Spruce		0.056 (0.034)		0.639 (0.775)		0.497 (0.579)	
Pine		0.136 (0.037)		1.115 (0.789)		1.777 (0.627)	
Site	2		0.140		0.052		0.013
P2		-0.017 (0.035)		0.402 (0.801)		0.470 (0.590)	
P3		-0.042 (0.036)		0.870 (0.773)		0.399 (0.599)	
Random effects			Year (Tree)		Year (Tree) + Tree		Year (Tree)
$R^2_{\text{(marginal)}}$			0.770		0.937		0.949
$R^2_{\text{(conditional)}}$			0.798		0.941		0.953

df, degrees of freedom; $R^2_{\text{(marginal)}}$, proportion of variance explained by fixed factors; $R^2_{\text{(conditional)}}$, proportion of variance explained by both the fixed and random factors.

Fixed effects: number of cells (nC), cell division rates (eR), cell residence times for enlargement (dE), wall thickening (dW), species (silver fir, Norway spruce and Scots pine) and site (P1, P2, P3). Random effect 'Year (Tree)' denotes that Year is nested in Tree. Significant fixed-effect estimates are highlighted in bold. SEs of the estimates are given in parentheses. Intercept estimates correspond to fir at the high-elevation site (P1). Sum-of-squares (SS) relates to the variance explained by each fixed factor.

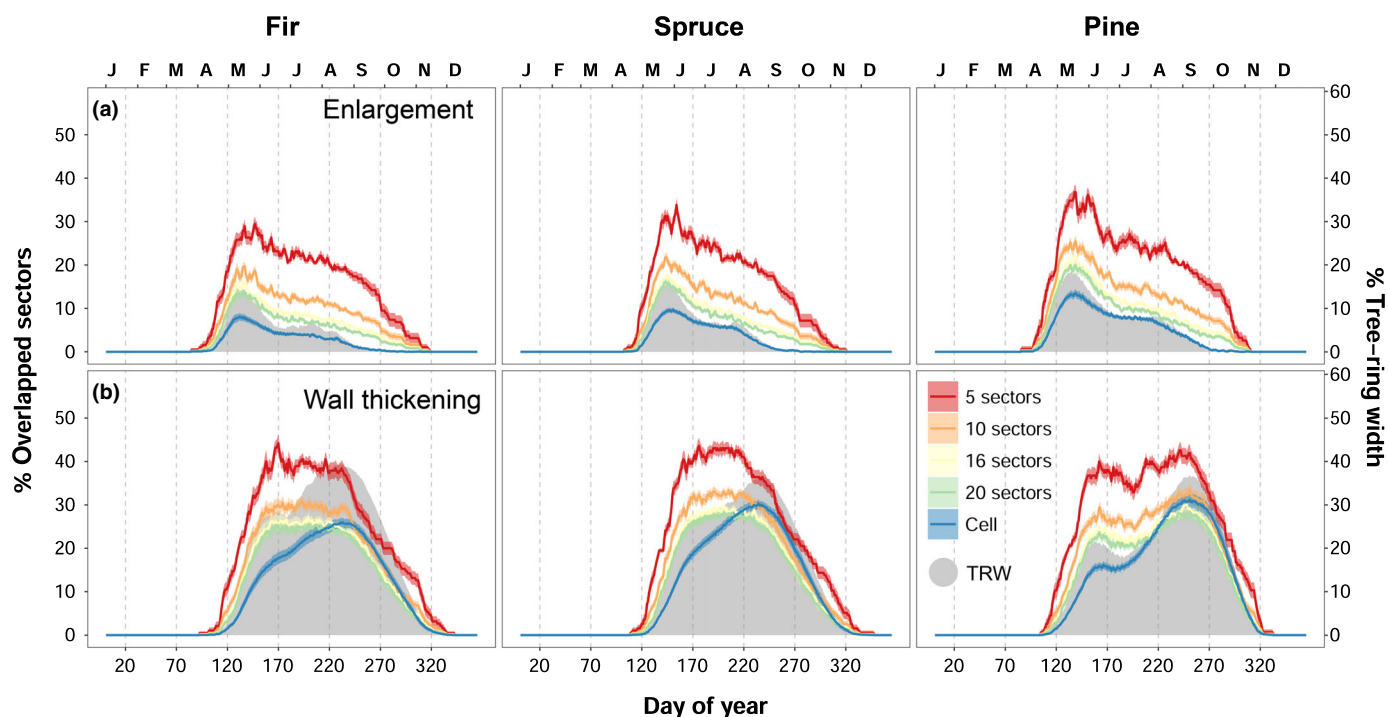


Fig. 4 Daily variation of the percentage of sectors containing enlarging (a) and wall-thickening (b) cells in silver fir, Norway spruce and Scots pine. Lines of different colours represent simulations for 5–20 regular sectors and at the cell level. The mean \pm SE is shown for each species. The grey area represents the mean percentage of the tree-ring width (TRW) containing cells in enlargement (a) and wall thickening (b) for each study species according to the final annual increment.

thickening was stable throughout the growing season across years, being on average 74% in fir, 82% in spruce and 86% in pine. Conversely, the enlargement of sectors 5–9 tended to occur in

different periods each year (Fig. 5b), albeit with noticeable differences among species (Table 3; Fig. 5b). Similar trends were noted for 10, 16 and 20 sector divisions, whereas higher values

Table 2 Generalized linear mixed models for the maximum percentage of overlapped sectors ($n = 108$ rings).

Fixed effects	df	Enlargement		Wall thickening	
		Est (SE)	SS	Est (SE)	SS
Intercept		41.274 (1.198)		56.819 (2.068)	
RCN	1	-2.502 (0.141)	44.056	-2.079 (0.261)	1.747
Mean CD	1	0.021 (0.229)	0.105	-0.397 (0.307)	0.583
Mean CWT	1			2.297 (0.274)	1.397
Sector frequency	4		81.638		15.877
10 sectors		-14.682 (1.074)		-14.094 (0.928)	
16 sectors		-20.448 (1.010)		-19.002 (0.890)	
20 sectors		-22.075 (0.993)		-20.696 (0.877)	
Cell		-29.539 (0.934)		-22.910 (0.862)	
Species	2		2.788		0.259
Spruce		-0.354 (0.432)		0.072 (0.608)	
Pine		3.385 (0.583)		-1.336 (0.699)	
Site	2		0.023		0.389
P2		-0.210 (0.520)		2.000 (0.726)	
P3		0.090 (0.425)		-0.811 (0.664)	
Random effects			Year		Year
$R^2_{\text{(marginal)}}$			0.765		0.706
$R^2_{\text{(conditional)}}$			0.767		0.716

df, degrees of freedom; $R^2_{\text{(marginal)}}$, proportion of variance explained by fixed factors; $R^2_{\text{(conditional)}}$, proportion of variance explained by both the fixed and random factors.

Fixed effects: ring cell number (RCN), mean cell diameter of the ring (CD), mean cell-wall thickness (CWT), wall thickening (dW), sector frequency (5, 10, 16 and 20 sectors, and cell level), species (silver fir, Norway spruce and Scots pine) and site (P1, P2, P3). Random effect: 'Year'. Significant fixed-effect estimates are highlighted in bold. SEs of the estimates are given in parentheses. Intercept estimates correspond to fir at the high-elevation site (P1) with a ring divided into five regular sectors. Sum-of-squares (SS) relates to the variance explained by each fixed factor.

were found for five divisions, especially during enlargement (Figs S7–S9).

Models indicated that the beginning of enlargement (bE_1) had a significant effect on interannual stability (Table 3), but not on inter-tree synchronicity, with lower inter-tree variability for bE_1 than for dSE_1 and dSW_1 (Table S3). High nC per sector implied less synchronous enlargement, but more synchronous and stable sector wall-thickening. During enlargement, eR and dE had, respectively, a negative and positive impact in both inter-tree synchronicity and interannual stability (Table 3). During wall thickening, inter-tree synchronicity was negatively affected by both eR and dW , but inverse relationships were found for interannual stability. The observed decline in synchronicity and stability as sector frequency increased from 5 to 20 sectors was much stronger for enlargement than for wall thickening (Table 3; Fig. 6). Pines showed the most stable enlargement and wall-thickening time intervals (Table 3; Fig. S6), whereas differences across sites were observed only for enlargement. The variance explained by the fixed factors was limited, however, especially for wall thickening (low marginal R^2 , Table 3).

Discussion

Variable time resolution, inter-tree synchronicity and interannual stability of sector formation along the tree ring

In a ring divided into 10 regular sectors, the time taken by the last-formed sectors was three-fold that of the first ones (Fig. 3). Variable sector timespans in intra-ring series entails that climate information is integrated in wood in a nonlinear way, as pointed out by observational tree-ring studies (Schollaen *et al.*, 2014; Soudant *et al.*, 2016), and process-based models (Ogée *et al.*, 2009; Eglin *et al.*, 2010; Belmecheri *et al.*, 2018). However, time resolution also depends on the variable time overlapping between consecutive sectors along the growing season (Fig. 4), which additionally confirms that the information contained in different sectors is not recorded in separate time windows. Large time overlapping across sectors accounts for widespread responses of cell diameter and wall thickness to climate across intra-ring sectors, as reported in dendroanatomy studies (Carrer *et al.*, 2016, 2017; Pacheco *et al.*, 2018), and agrees with high correlations between chronologies obtained from adjacent sectors (Castagneri *et al.*, 2017; Belokopytova *et al.*, 2019).

High inter-tree synchronicity and interannual stability of sector formation is desirable to build chronologies of intra-ring traits. The first and last sectors from different trees were formed in coincident time intervals (inter-tree sector synchronicity, Fig. 5a), but this pattern was maintained in intermediate sectors for wall thickening only. Similar results were obtained for equivalent sectors within the same tree across the three study years (interannual sector stability; Fig. 5b). High synchronicity during the last sector enlargement concurred with the high interseries correlation noted in dendroanatomy studies for latewood sectors (Castagneri *et al.*, 2017; Belokopytova *et al.*, 2019). Likewise, the high interannual coefficient of variation in cell lumen area and wall thickness reported by Belokopytova *et al.* (2019) in transition wood would be compatible with the lower stability for intermediate sectors noted here during enlargement.

Mechanisms controlling timespan, overlapping, synchronicity and stability of tree-ring sectors

The duration of sector formation was a result of the combination of xylogenesis traits (cell division rates and residence times in enlargement and wall thickening) and the number of cells per sector (nC). The total duration of sector formation (dSX) was determined mainly by the time taken by tracheids to enlarge (dE) and, to a greater extent, build and lignify their walls (dW). The high importance of dW may be attributed to the fact that, except for the first-formed tracheids, wall thickening takes much longer than cell enlargement (Skene, 1972; Cuny *et al.*, 2014; Balducci *et al.*, 2016; Buttò *et al.*, 2019; Vieira *et al.*, 2020). The significant effect of nC on sector timespan suggests that regular sectoring would exacerbate differences in duration across sectors, with more cell formation intervals being accumulated in sectors containing latewood-like cells (Fig. 3b). This would be aggravated by low cell division rates (eR) occurring at the end of the growing

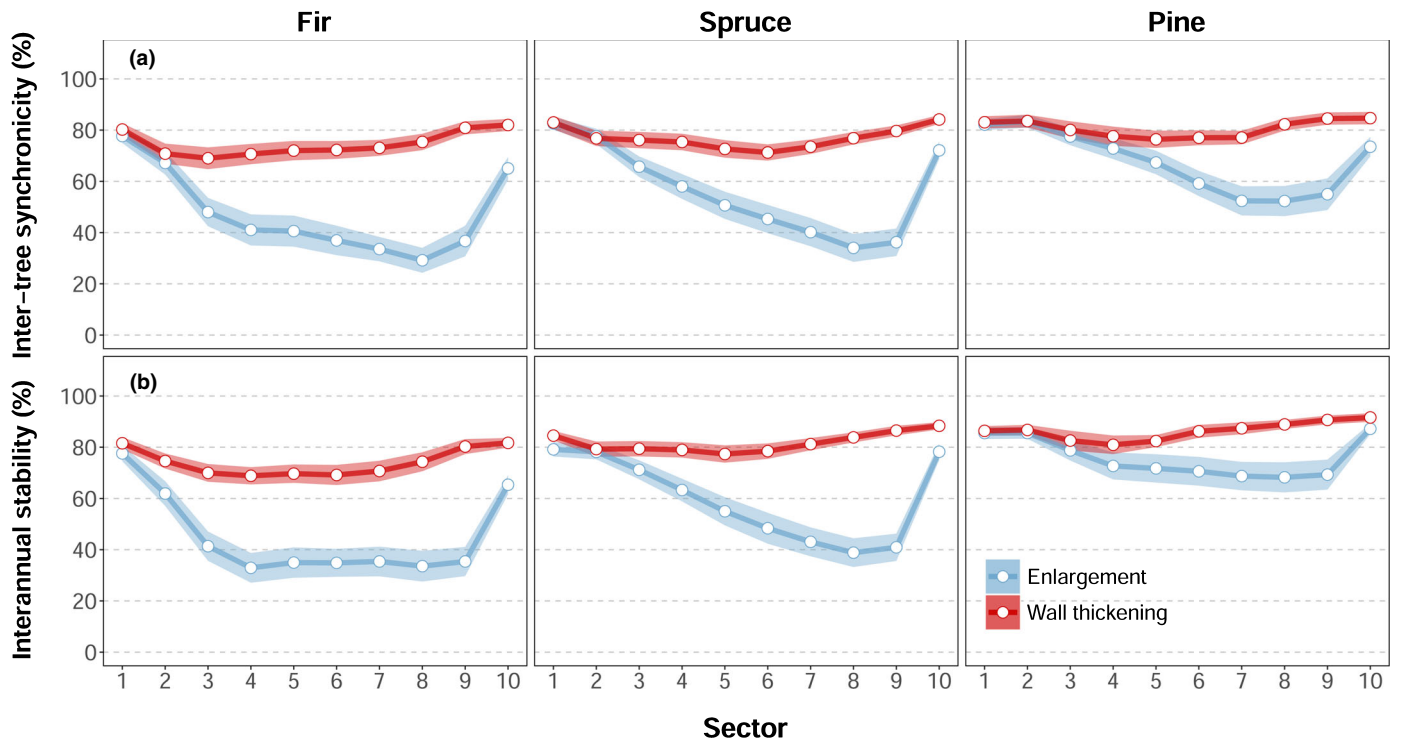


Fig. 5 Mean inter-tree synchronicity (a) and interannual stability (b) \pm SE for 10 sectors during cell enlargement (blue) and wall thickening (red) in silver fir, Norway spruce and Scots pine.

Table 3 Linear mixed-effects models for inter-tree synchronicity and interannual stability in tree-ring sectors during enlargement and wall thickening.

Fixed effects	Inter-tree synchronicity ($n = 108$ rings)				Interannual stability ($n = 102$ rings)			
	Enlargement		Wall thickening		Enlargement		Wall thickening	
	Est (SE)	SS	Est (SE)	SS	Est (SE)	SS	Est (SE)	SS
Intercept	70.452 (4.084)		76.167 (3.128)		58.670 (4.471)		69.308 (3.187)	
bE_1	2.723 (2.255)	1082	1.065 (1.787)	83	6.884 (2.487)	4847	3.675 (1.810)	799
nC	-2.752 (0.710)	11 154	3.712 (0.431)	17 222	0.749 (0.672)	787	3.832 (0.403)	17 537
eR	-5.655 (0.541)	81 121	-2.724 (0.306)	18 422	-5.640 (0.506)	78 746	0.989 (0.282)	2386
dE	4.814 (0.527)	62 003	-1.250 (0.304)	3935	5.325 (0.511)	68 626	-0.107 (0.291)	26
dW			-1.407 (0.250)	7338			0.756 (0.233)	2041
Sector frequency		256 548		4949		126 391		3525
10 sectors	-19.992 (1.750)		-1.072 (1.008)		-13.634 (1.677)		-0.304 (0.956)	
16 sectors	-30.981 (1.923)		-3.031 (1.126)		-22.011 (1.852)		-1.847 (1.072)	
20 sectors	-35.065 (1.993)		-3.932 (1.172)		-25.264 (1.922)		-2.873 (1.118)	
Species		2797		1356		12 763		4300
Spruce	2.651 (4.866)		3.025 (3.855)		4.626 (5.458)		5.627 (3.972)	
Pine	8.738 (4.511)		8.601 (3.562)		22.507 (5.056)		17.295 (3.673)	
Site		3302		384		6978		351
P2	-0.023 (4.799)		-4.721 (3.802)		0.378 (5.514)		-3.834 (4.013)	
P3	7.865 (4.446)		-3.341 (3.514)		13.951 (5.037)		4.841 (3.662)	
Random effects		Year (Tree)		Year (Tree)		Year (Tree)		Year (Tree)
$R^2_{(marginal)}$		0.176		0.078		0.248		0.148
$R^2_{(conditional)}$		0.423		0.508		0.531		0.586

$R^2_{(marginal)}$, proportion of variance explained by fixed factors; $R^2_{(conditional)}$, proportion of variance explained by both the fixed and random factors. Fixed effects: date of the beginning of the first sector enlargement (bE_1), number of cells (nC), cell division rates (eR), cell residence times for enlargement (dE), wall thickening (dW), sector frequency (5, 10, 16 and 20 sectors), species (silver fir, Norway spruce and Scots pine), and site (P1, P2, P3). Random effect 'Year (Tree)' denotes that Year is nested in Tree. Significant fixed-effect estimates are highlighted in bold. SEs of the estimates are given in parentheses. Intercept estimates correspond to fir at the high-elevation site (P1).

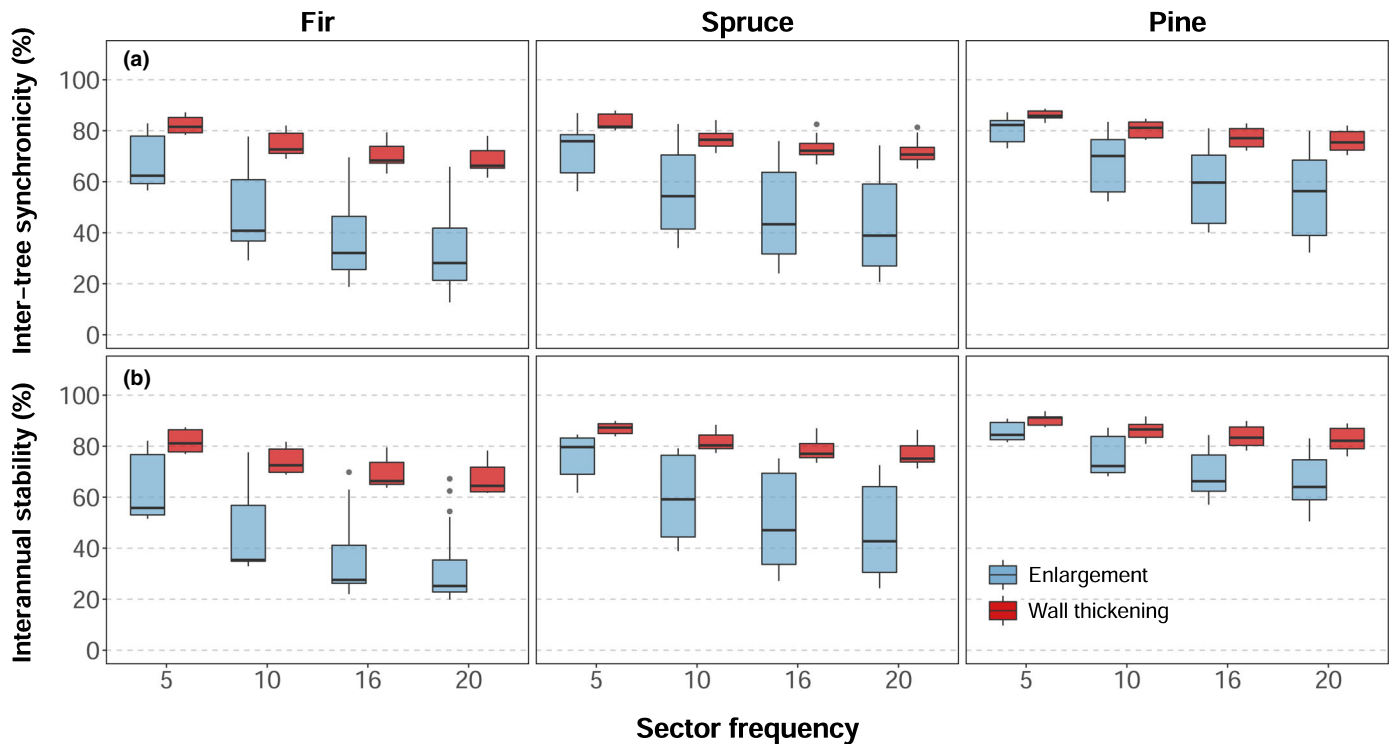


Fig. 6 Variation in mean inter-tree synchronicity (a) and interannual stability (b) during cell enlargement (blue) and wall thickening (red) for rings divided into 5, 10, 16 and 20 regular sectors in silver fir, Norway spruce and Scots pine. Horizontal lines within boxes represent median values, lower and upper box limits correspond to the first and third quartiles, vertical lines mark the most extreme values observed within 1.5 times the interquartile range, and grey dots indicate outliers.

season (Fig. 3c), which would contribute to the extension of the last sector duration. Despite their narrower rings and sectors, pines showed relatively longer sector enlargement, which could be attributed to their overall low eR compared to firs and spruces. Therefore, when comparing different species, thinner ring widths do not necessarily entail shorter ring or sector formation periods.

Consecutive sector overlapping varied between phases, with the daily amount of simultaneous wall-thickening wood being $\leq 27.3\%$ higher than that of enlargement. Longer dSW than dSE across sectors would account for the higher overlapping noted for wall thickening (Fig. 4). This is consistent with the positive effect of mean CWT on overlapping, as thicker walls may be associated with longer wall-thickening periods (Cuny & Rathgeber, 2016; Buttò *et al.*, 2019). The observed decline in dSE and dSW with nC also may explain the reduction in maximum sector overlapping after increasing sector frequency from 5 to 16 sectors (Figs S4, S5). In addition, sector overlapping was magnified in narrow rings (Table 2), which is consistent with RCN being inversely associated with dE. It is worth noting that pines showed narrower rings, longer dSE and more overlapped sectors than the other species. However, narrow rings also resulted from low eR, which should limit accumulation of contemporary cells. Indeed, overlapping peaked in early summer (Fig. 4), the time when cell division rates are maximal in temperate conifers (Cuny *et al.*, 2012; Gričar *et al.*, 2014). This suggests that maximum overlapping depends on the duration of sector formation rather than on eR, even though the latter may control seasonal patterns of sector overlapping.

Sector timespans played a major role in shaping inter-tree synchronicity and interannual stability (Table 3). Sectors formed under low eR and long dE had more synchronous and stable enlargement time intervals, whereas sectors having more cells had a more synchronous and stable wall thickening. Pines had a more stable growth than firs and spruces probably because of their longer dSE (Figs 3, 5). This also is consistent with the decline in synchronicity and stability as sector frequency increased (Fig. 6). Moreover, the higher synchronicity and stability for wall thickening than for enlargement in intermediate sectors is consistent with their dSW being longer than dSE (Fig. 5). However, highly synchronic growth in the first-formed sectors is at odds with their low durations, rather reflecting the low inter-tree variability in xylem growth resumption (bE_1). In cold areas, a tight control of the timing of growth reactivation may be critical to avoid exposition of the new tissues to frost damage (Begum *et al.*, 2012), whereby cambial activity may resume within a narrow range of temperatures (Gričar *et al.*, 2014). Under warmer climates, more asynchronous and variable sector formation could be expected, however, with high inter-tree and interannual variation in wood phenology being reported for tropical (De Mil *et al.*, 2019) and Mediterranean sites (Fernández-de-Uña *et al.*, 2018; Vieira *et al.*, 2020). Indeed, we found that interannual changes in bE_1 had a significant impact on stability. Nonetheless, although warming-induced changes in spring phenology could weaken wood formation synchronisms (Yang *et al.*, 2017), more extreme events later in the season could trigger more synchronic interannual growth patterns across populations (Shestakova *et al.*, 2016).

Implications of developmental constraints on tree-ring sectoring and future research applications

Cell-wall material being deposited on sectors over long and highly overlapped time intervals could smoothen intra-annual fluctuations in wood biomass-related traits compared to volume-related ones. This points out the importance of identifying whether a trait is recorded during enlargement or wall thickening. Wood anatomy traits such as cell diameter (CD) are associated with changes in wood volume, which partially supports the use of dendrometers to date dendroanatomy series (Pacheco *et al.*, 2018). Yet, although CD is determined by conditions affecting cell enlargement (Cuny *et al.*, 2014), CWT and wood microdensity are determined by both cell diameter and conditions affecting wall thickening (Cuny *et al.*, 2014, 2019; Wilkinson *et al.*, 2015; Björklund *et al.*, 2017; Castagneri *et al.*, 2017).

Tree-ring isotope ratios are expected to be recorded during wall thickening and lignification (Monson *et al.*, 2018), when most of the woody biomass is incorporated (Cuny *et al.*, 2015; Locosselli & Buckeridge, 2017). Unlike CD, CWT or wood microdensity, C isotope signal originates in the leaf, long before its incorporation into the ring, being also affected by fractionation processes occurring during sugar transport and storage (Barbour *et al.*, 2002; Gessler *et al.*, 2014). Before becoming structural compounds, young sugars are mixed with multi-year C reserves (Hartmann & Trumbore, 2016), the contribution to growth of which varies seasonally (Helle & Schleser, 2004). This probably mitigates the relative importance of wood cell formation time intervals on the tree-ring isotope signature. Although Treydte *et al.* (2014) dated whole-wood $\delta^{18}\text{O}$ series from larch using the timings of cell enlargement, Fonti *et al.* (2018) considered the entire cell formation to date whole-wood $\delta^{13}\text{C}$ records in Scots pine. Belmecheri *et al.* (2018), however, found that modelled $\delta^{18}\text{O}$ values in cellulose from false rings of ponderosa pine were more accurate when associated with the wall-thickening period. The recording period also may vary between whole wood and cellulose (Shestakova & Martínez-Sancho, 2021). Cellulose and lignin may not have the same deposition times (Donaldson, 1991), especially in sectors formed after abrupt cooling events, which may delay or hamper lignification (Piermattei *et al.*, 2020). Yet, distinction between dates of wall-thickening and lignification is rare in xylogensis studies, as it was our case, whereby the whole-wood isotope recording time interval probably would correspond better to the wall-thickening timings from xylogensis datasets than that of cellulose. Hence, the application of advanced microscopy techniques enabling a better distinction between cellulose and lignin deposition might allow the incorporation of the cellulose isotopic signal to be dated more accurately.

Study trees showed a high number of sectors being formed simultaneously in early summer (Fig. 4), which is consistent with maximum rates of cell division occurring around the summer solstice (Cuny *et al.*, 2012; Gričar *et al.*, 2014; Balducci *et al.*, 2016). This is in line with TRW series being highly responsive to atmospheric conditions in early summer in temperate and boreal conifers (Carrer *et al.*, 2016, 2017; Belokopytova *et al.*, 2019). Similar relationships were reported for $\delta^{13}\text{C}$ records (Soudant *et*

al., 2016; Szejner *et al.*, 2016; Fonti *et al.*, 2018), suggesting that the strength of the isotope signal may depend not only on the intensity of the physiological response at the source (e.g. photosynthetic C isotope discrimination), but also on the amount of living tissue at each time. Thus, although early-summer signals are amplified, responses occurring later in the season could be attenuated in annually resolved isotope records, with stressful conditions halting cambial activity remaining likely undetected (Pflug *et al.*, 2015). This is of particular importance in dry Mediterranean sites, where summer drought may lead to a more complex bimodal growth and earlier maximum rates of cell division than in temperate sites (Fernández-de-Uña *et al.*, 2018; Vieira *et al.*, 2020). However, at the intra-annual level, the observed low overlapping in the first- and last-formed sectors could elicit a more distinct signal than in intermediate sectors. This may be the case for redwood rings that show, only at the ring boundary, enriched $\delta^{18}\text{O}$ values associated with summer fog (Roden *et al.*, 2009). In addition, the first-formed sector often contains a similar isotope signal as the previous-ring last sector, which has been attributed to the high reliance of growth on internal C and water reserves at the beginning of the growing season (Helle & Schleser, 2004; Gessler *et al.*, 2014; Treydte *et al.*, 2014).

Increasing spatial resolution enables a reduction of sector timespan and thus overlapping (Fig. 4). Nevertheless, high sector frequency may exacerbate asynchrony across trees, particularly during cell enlargement (Fig. 6). In addition, our results convey that the maximum time resolution ultimately is constrained by the number of contemporaneous living cells, rather than by the instrumental capacity to increase spatial measuring resolution. In this regard, we found an optimal sector frequency in temperate conifers of *c.* 15 regular sectors for rings with 25–200 cells in a radial file (700–6400 μm wide) (Fig. S4). However, the effect of RCN on sector overlapping suggests that the optimal number of sectors would vary for either narrower or wider rings than those observed in our study. Moreover, our observations cannot be generalized to warmer environments, where trees often show complex intra-annual growth patterns and high interannual growth variation (De Mil *et al.*, 2019; Vieira *et al.*, 2020; Ziaco, 2020). Although irregular sectoring based on changes in cell morphology could be appropriate in species with complex intra-ring patterns, equivalence between sectors across trees and years would be uncertain (De Micco *et al.*, 2012). Therefore, irregular sectoring would require previous knowledge of the associations between the timing of wood formation processes and the characteristics of tree rings to minimize subjectivity.

Conclusions

Dendrochronological records are crucial to understand long-term tree functional responses to environmental cues, but their reliability in deciphering intra-annual signals is still unclear because intra-ring sector formation dates cannot be inferred easily in mature rings. Retrospective dating of intra-ring sectors is challenged by the variable time resolution for cell enlargement and wall thickening, but also across successive sectors owing to differences in their formation timespan and variable level of

overlapping. Intra-ring chronologies based on enlargement-related traits have inherently higher time resolution, whereas those based on wall-thickening-related traits are more reliable as a result of their higher level of synchronization among trees and stability over the years. However, a similar reliability could be obtained for enlargement-related traits measured near the ring boundaries. Notwithstanding this, a more mechanistic understanding of xylogenesis phases and their structural consequences across species and environmental conditions is still needed to properly link wood formation processes (enlargement, wall thickening, lignification), intra-ring traits (isotopic composition, cell morphology) and the signals that they convey.


Acknowledgements


The authors thank: H. Cuny for collecting, preparing and observing wood formation and anatomy samples; SILVATECH (Silvatech, INRAE, 2018. Structural and functional analysis of tree and wood facility, doi: 10.15454/1.5572400113627854E12) from UMR 1434 SILVA; 1136 IAM, 1138 BEF and 4370 EA LERMAB from the research center INRAE Grand-Est Nancy for its contribution to wood sample collection (E. Cornu, E. Farré, C. Freyburger, P. Gelhaye, and A. Mercanti) and preparation (M. Harroué); and the editor and two referees for their suggestions. This work was supported by a grant overseen by the French National Research Agency (ANR) as part of the ‘Investissements d’Avenir’ program (ANR-11-LABX-0002-01, Laboratory of Excellence ARBRE), and by the program ‘Soutien aux jeunes chercheurs’ (18_GE5_018) funded by the Conseil Régional Grand Est (France). GPL benefited from a Xunta de Galicia–Fulbright fellowship (ED481B2019/108) and is grateful to Xunta de Galicia for the recognition of the Research Competitive Reference Group GI-1809 BIOAPLIC (ED431C 2019/07). LFU was a recipient of an AgreenSkills+ fellowship funded by the EU’s Seventh Framework Program under grant agreement no. FP7-609398 (AgreenSkills+ contract).


Author contributions


CBKR, SP and GP-L conceived and designed the research; and GP-L, CBKR, LF-U and SP participated in analyzing the data and writing the manuscript.

ORCID

Laura Fernández-de-Uña  <https://orcid.org/0000-0001-8136-2545>

Gonzalo Pérez-de-Lis  <https://orcid.org/0000-0002-7913-2190>

Stéphane Ponton  <https://orcid.org/0000-0002-4821-2438>

Cyrille B. K. Rathgeber  <https://orcid.org/0000-0001-7359-8320>

Data availability

Data are available on request from the authors.

References

- Balducci L, Cuny HE, Rathgeber CBK, Deslauriers A, Giovannelli A, Rossi S. 2016. Compensatory mechanisms mitigate the effect of warming and drought on wood formation. *Plant, Cell & Environment* 39: 1338–1352.
- Barbour MM, Walcroft AS, Farquhar GD. 2002. Seasonal variation in $\delta^{13}\text{C}$ and $\delta^{18}\text{O}$ of cellulose from growth rings of *Pinus radiata*. *Plant, Cell & Environment* 25: 1483–1499.
- Bates D, Mächler M, Bolker BM, Walker SC. 2015. Fitting linear mixed-effects models using lme4. *Journal of Statistical Software* 67: 1–48.
- Begum S, Shibagaki M, Furusawa O, Nakaba S, Yamagishi Y, Yoshimoto J, Jin HO, Sano Y, Funada R. 2012. Cold stability of microtubules in wood-forming tissues of conifers during seasons of active and dormant cambium. *Planta* 235: 165–179.
- Belmecheri S, Wright WE, Szejner P, Morino KA, Monson RK. 2018. Carbon and oxygen isotope fractionations in tree rings reveal interactions between cambial phenology and seasonal climate. *Plant, Cell & Environment* 41: 2758–2772.
- Belokopytova LV, Babushkina EA, Zhirnova DF, Panyushkina IP, Vaganov EA. 2019. Pine and larch tracheids capture seasonal variations of climatic signal at moisture-limited sites. *Trees – Structure and Function* 33: 227–242.
- Björklund J, Seftigen K, Schweingruber F, Fonti P, von Arx G, Bryukhanova MV, Cuny HE, Carrer M, Castagneri D, Frank DC. 2017. Cell size and wall dimensions drive distinct variability of earlywood and latewood density in Northern Hemisphere conifers. *New Phytologist* 216: 728–740.
- Bouriaud O, Leban JM, Bert D, Deleuze C. 2005. Intra-annual variations in climate influence growth and wood density of Norway spruce. *Tree Physiology* 25: 651–660.
- Buttò V, Rossi S, Deslauriers A, Morin H. 2019. Is size an issue of time? Relationship between the duration of xylem development and cell traits. *Annals of Botany* 123: 1257–1265.
- Carrer M, Brunetti M, Castagneri D. 2016. The imprint of extreme climate events in century-long time series of wood anatomical traits in high-elevation conifers. *Frontiers in Plant Science* 7: 683.
- Carrer M, Castagneri D, Prendin AL, Petit G, von Arx G. 2017. Retrospective analysis of wood anatomical traits reveals a recent extension in tree cambial activity in two high-elevation conifers. *Frontiers in Plant Science* 8: 737.
- Castagneri D, Fonti P, Von Arx G, Carrer M. 2017. How does climate influence xylem morphogenesis over the growing season? Insights from long-term intra-ring anatomy in *Picea abies*. *Annals of Botany* 119: 1011–1020.
- Cuny HE, Fonti P, Rathgeber CBK, von Arx G, Peters RL, Frank DC. 2019. Couplings in cell differentiation kinetics mitigate air temperature influence on conifer wood anatomy. *Plant, Cell & Environment* 42: 1222–1232.
- Cuny HE, Rathgeber CBK. 2016. Xylogenesis: coniferous trees of temperate forests are listening to the climate tale during the growing season but only remember the last words! *Plant Physiology* 171: 306–317.
- Cuny HE, Rathgeber CBK, Frank D, Fonti P, Fournier M. 2014. Kinetics of tracheid development explain conifer tree-ring structure. *New Phytologist* 203: 1231–1241.
- Cuny HE, Rathgeber CBK, Frank D, Fonti P, Mäkinen H, Prislán P, Rossi S, del Castillo EM, Campelo F, Vavrčík H *et al.* 2015. Woody biomass production lags stem-girth increase by over one month in coniferous forests. *Nature Plants* 1: 15160.
- Cuny HE, Rathgeber CBK, Kiessé TS, Hartmann FP, Barbeito I, Fournier M. 2013. Generalized additive models reveal the intrinsic complexity of wood formation dynamics. *Journal of Experimental Botany* 64: 1983–1994.
- Cuny HE, Rathgeber CBK, Lebourgeois F, Fortin M, Fournier M. 2012. Life strategies in intra-annual dynamics of wood formation: example of three conifer species in a temperate forest in north-east France. *Tree Physiology* 32: 612–625.
- De Micco V, Battipaglia G, Brand WA, Linke P, Saurer M, Aronne G, Cherubini P. 2012. Discrete versus continuous analysis of anatomical and $\delta^{13}\text{C}$ variability in tree rings with intra-annual density fluctuations. *Trees – Structure and Function* 26: 513–524.
- De Mil T, Hubau W, Angoboy Ilondea B, Rocha Vargas MA, Boeckx P, Steppe K, Van Acker J, Beeckman H, Van Den Bulcke J. 2019. Asynchronous leaf and cambial phenology in a tree species of the Congo Basin requires space-time conversion of wood traits. *Annals of Botany* 124: 245–253.

- Donaldson LA. 1991. Seasonal changes in lignin distribution during tracheid development in *Pinus radiata* D. Don. *Wood Science and Technology* 25: 15–24.
- Eglin T, Francois C, Michelot A, Delpierre N, Damesin C. 2010. Linking intra-seasonal variations in climate and tree-ring $\delta^{13}\text{C}$: a functional modelling approach. *Ecological Modelling* 221: 1779–1797.
- Fernández-de-Uña L, Aranda I, Rossi S, Fonti P, Cañellas I, Gea-Izquierdo G. 2018. Divergent phenological and leaf gas exchange strategies of two competing tree species drive contrasting responses to drought at their altitudinal boundary. *Tree Physiology* 38: 1152–1165.
- Fonti MV, Vaganov EA, Wirth C, Shashkin AV, Astrakhantseva NV, Schulze E-D. 2018. Age-effect on intra-annual $\delta^{13}\text{C}$ -variability within scots pine tree-rings from Central Siberia. *Forests* 9: 364.
- Fritts HC. 1976. *Tree rings and climate*. London, UK: Academic Press.
- Gessler A, Ferrio JP, Hommel R, Treydte K, Werner RA, Monson RK. 2014. Stable isotopes in tree rings: towards a mechanistic understanding of isotope fractionation and mixing processes from the leaves to the wood. *Tree Physiology* 34: 796–818.
- Gričar J, Prisljan P, Gryc V, Vavričik H, de Luis M, Cufar K. 2014. Plastic and locally adapted phenology in cambial seasonality and production of xylem and phloem cells in *Picea abies* from temperate environments. *Tree Physiology* 34: 869–881.
- Hartmann H, Trumbore S. 2016. Understanding the roles of nonstructural carbohydrates in forest trees – from what we can measure to what we want to know. *New Phytologist* 211: 386–403.
- Helle G, Schleser GH. 2004. Beyond CO_2 -fixation by Rubisco – an interpretation of $^{13}\text{C}/^{12}\text{C}$ variations in tree rings from novel intra-seasonal studies on broad-leaf trees. *Plant, Cell & Environment* 27: 367–380.
- Hothorn T, Bretz F, Westfall P. 2008. Simultaneous inference in general parametric models. *Biometrical Journal* 50: 346–363.
- Kuznetsova A, Brockhoff PB, Christensen RHB. 2017. LMERTEST package: tests in linear mixed effects models. *Journal of Statistical Software* 82: 1–26.
- Locosselli GM, Buckeridge MS. 2017. Dendrochemistry, a missing link to further understand carbon allocation during growth and decline of trees. *Trees – Structure and Function* 31: 1745–1758.
- Monson RK, Szejner P, Belmecheri S, Morino KA, Wright WE. 2018. Finding the seasons in tree ring stable isotope ratios. *American Journal of Botany* 105: 1–3.
- Nakagawa S, Schielzeth H. 2013. A general and simple method for obtaining R^2 from generalized linear mixed-effects models. *Methods in Ecology and Evolution* 4: 133–142.
- Ogée J, Barbour MM, Wingate L, Bert D, Bosc A, Stievenard M, Lambrot C, Pierre M, Bariac T, Loustau D *et al.* 2009. A single-substrate model to interpret intra-annual stable isotope signals in tree-ring cellulose. *Plant, Cell & Environment* 32: 1071–1090.
- Pacheco A, Camarero JJ, Ribas M, Gazol A, Gutierrez E, Carrer M. 2018. Disentangling the climate-driven bimodal growth pattern in coastal and continental Mediterranean pine stands. *Science of the Total Environment* 615: 1518–1526.
- Pflug EE, Siegwolf R, Buchmann N, Dobbertin M, Kuster TM, Günthardt-Goerg MS, Arend M, Guenthardt-Goerg MS, Arend M, Günthardt-Goerg MS *et al.* 2015. Growth cessation uncouples isotopic signals in leaves and tree rings of drought-exposed oak trees. *Tree Physiology* 35: 1095–1105.
- Piermattei A, Crivellaro A, Krusic PJ, Esper J, Vitek P, Oppenheimer C, Felhofer M, Gierlinger N, Reinig F, Urban O *et al.* 2020. A millennium-long ‘Blue Ring’ chronology from the Spanish Pyrenees reveals severe ephemeral summer cooling after volcanic eruptions. *Environmental Research Letters* 15: 124016.
- Popkova MI, Vaganov EA, Shishov VV, Babushkina EA, Rossi S, Fonti MV, Fonti P. 2018. Modeled tracheidograms disclose drought influence on *Pinus sylvestris* tree-rings structure from Siberian forest-steppe. *Frontiers in Plant Science* 9: 1–12.
- Pritzkow C, Heinrich I, Grudd H, Helle G. 2014. Relationship between wood anatomy, tree-ring widths and wood density of *Pinus sylvestris* L. and climate at high latitudes in northern Sweden. *Dendrochronologia* 32: 295–302.
- Pya N, Wood SN. 2014. Shape constrained additive models. *Statistics and Computing* 25: 543–559.
- R Core Team. 2017. *R: a language and environment for statistical computing*. 1: 409. Vienna, Austria: R Foundation for Statistical Computing.
- Rathgeber CBK, Cuny HE, Fonti P. 2016. Biological basis of tree-ring formation: a crash course. *Frontiers in Plant Science* 7: 1–7.
- Rathgeber CBK, Santenoise P, Cuny HE. 2018. CAVIAR: an R package for checking, displaying and processing wood-formation-monitoring data. *Tree Physiology* 38: 1246–1260.
- Roden JS, Johnstone JA, Dawson TE. 2009. Intra-annual variation in the stable oxygen and carbon isotope ratios of cellulose in tree rings of coast redwood (*Sequoia sempervirens*). *Holocene* 19: 189–197.
- Schollaen K, Heinrich I, Helle G. 2014. UV-laser-based microscopic dissection of tree rings – a novel sampling tool for $\delta^{13}\text{C}$ and $\delta^{18}\text{O}$ studies. *New Phytologist* 201: 1045–1055.
- Schollaen K, Heinrich I, Neuwirth B, Krusic PJ, D’Arrigo RD, Karyanto O, Helle G. 2013. Multiple tree-ring chronologies (ring width, $\delta^{13}\text{C}$ and $\delta^{18}\text{O}$) reveal dry and rainy season signals of rainfall in Indonesia. *Quaternary Science Reviews* 73: 170–181.
- Shestakova TA, Gutiérrez E, Kiryanov AV, Camarero JJ, Génova M, Knorre AA, Linares JC, Resco de Dios V, Sánchez-Salguero R, Voltas J. 2016. Forests synchronize their growth in contrasting Eurasian regions in response to climate warming. *Proceedings of the National Academy of Sciences, USA* 113: 662–667.
- Shestakova TA, Martínez-Sancho E. 2021. Stories hidden in tree rings: a review on the application of stable carbon isotopes to dendrosciences. *Dendrochronologia* 65: 125789.
- Skene DS. 1972. The kinetics of tracheid development in *Tsuga canadensis* Carr. and its relation to tree vigour. *Annals of Botany* 36: 179–187.
- Soudant A, Loader NJ, Bäck J, Levula J, Kljun N. 2016. Intra-annual variability of wood formation and $\delta^{13}\text{C}$ in tree-rings at Hyttälä, Finland. *Agricultural and Forest Meteorology* 224: 17–29.
- Szejner P, Wright WE, Babst F, Belmecheri S, Trouet V, Leavitt SW, Ehleringer JR, Monson RK. 2016. Latitudinal gradients in tree ring stable carbon and oxygen isotopes reveal differential climate influences of the North American Monsoon System. *Journal of Geophysical Research: Biogeosciences* 121: 1978–1991.
- Szejner P, Wright WE, Belmecheri S, Meko D, Leavitt SW, Ehleringer JR, Monson RK. 2018. Disentangling seasonal and interannual legacies from inferred patterns of forest water and carbon cycling using tree-ring stable isotopes. *Global Change Biology* 24: 5332–5347.
- Szymczak S, Bräuning A, Häusser M, Garel E, Huneau F, Santoni S. 2019. The relationship between climate and the intra-annual oxygen isotope patterns from pine trees: a case study along an elevation gradient on Corsica, France. *Annals of Forest Science* 76: 76.
- Treydte K, Boda S, Graf Pannatier E, Fonti P, Frank D, Ullrich B, Saurer M, Siegwolf R, Battipaglia G, Werner W *et al.* 2014. Seasonal transfer of oxygen isotopes from precipitation and soil to the tree ring: source water versus needle water enrichment. *New Phytologist* 202: 772–783.
- Vieira J, Carvalho A, Campelo F. 2020. Tree growth under climate change: evidence from xylogenesis timings and kinetics. *Frontiers in Plant Science* 11: 90.
- Wilkinson S, Ogée J, Domec J-CC, Rayment M, Wingate L. 2015. Biophysical modelling of intra-ring variations in tracheid features and wood density of *Pinus pinaster* trees exposed to seasonal droughts. *Tree Physiology* 35: 305–318.
- Wood SN. 2006. *Generalized additive models: an introduction with R*. Boca Raton, FL, USA: Chapman and Hall/CRC Press.
- Yang B, He M, Shishov V, Tychkov I, Vaganov E, Rossi S, Ljungqvist FC, Bräuning A, Griebinger J. 2017. New perspective on spring vegetation phenology and global climate change based on Tibetan Plateau tree-ring data. *Proceedings of the National Academy of Sciences, USA* 114: 6966–6971.
- Ziaco E. 2020. A phenology-based approach to the analysis of conifers intra-annual xylem anatomy in water-limited environments. *Dendrochronologia* 59: 125662.

Supporting Information

Additional Supporting Information may be found online in the Supporting Information section at the end of the article.

Fig. S1 Temperature and daily precipitation at the study sites.

Fig. S2 Parameters for inter-tree synchronicity and interannual stability calculation.

Fig. S3 Duration of sector enlargement, wall thickening and entire formation per site and year.

Fig. S4 Maximum overlapping against ring cell number.

Fig. S5 Maximum overlapping across consecutive sectors.

Fig. S6 Inter-tree synchronicity and interannual stability per site and year.

Fig. S7 Inter-tree synchronicity and interannual stability for five sectors.

Fig. S8 Inter-tree synchronicity and interannual stability for 16 sectors.

Fig. S9 Inter-tree synchronicity and interannual stability for 20 sectors.

Table S1 List of acronyms, with their definitions and units.

Table S2 ANOVA of wood phenology and tree-ring structure parameters.

Table S3 Variability for the beginning of enlargement and first-sector durations.

Please note: Wiley Blackwell are not responsible for the content or functionality of any Supporting Information supplied by the authors. Any queries (other than missing material) should be directed to the *New Phytologist* Central Office.